Please cite this article in press as: Li et al., On the mechanism and voltage sensitivity of voltage-sensitive second harmonic probes: A case study of FM4-64, Biophysical Journal (2026), https://doi.org/10.1016/j.bpj.2026.07.006

Biophysical Journal
Article

Biophysical Society

On the mechanism and voltage sensitivity of voltage-sensitive second harmonic probes: A case study of FM4-64

Zhi Li,[1,5] Nelson Alonso Correa-Rojas,[1,5] Saranya Pullanchery,[1,4] Iwona Swiderska,[1] Arianna Marchioro,[1,*] and Sylvie Roke[1,2,3,*]

[1]Laboratory for Fundamental BioPhotonics (LBP), Institute of Bioengineering (IBI), School of Engineering (STI), École Polytechnique Fédérale de Lausanne (EPFL), Lausanne, Switzerland; [2]Institute of Materials Science and Engineering (IMX), School of Engineering (STI), École Polytechnique Fédérale de Lausanne (EPFL), Lausanne, Switzerland; and [3]Lausanne Centre for Ultrafast Science, École Polytechnique Fédérale de Lausanne (EPFL), Lausanne, Switzerland
[4]Present address: Department of Chemistry, TAMU 3255, 580 Ross St., College Station, TX, USA
[5]These authors contributed equally

ABSTRACT Voltage-sensitive dyes are frequently used to measure electrostatic potentials across (cell) membranes. Their use is based on the observed linear correlation between the second harmonic (SH) emission and an applied transmembrane potential. However, this intensity-to-potential conversion implicitly assumes a single, fixed dye orientation and a constant surface number density in the membrane, both taken to be independent of the local molecular environment. Here, we investigate whether these assumptions hold by imaging the SH response of a voltage-sensitive dye (FM4-64) in giant unilamellar vesicles. Using polarimetric SH microscopy, we determine changes in the orientational distribution parameter D and surface number density of FM4-64. We find that the orientational distribution of FM4-64 is influenced by the type of lipid and the charged state of the membrane. Zwitterionic saturated and unsaturated lipids display different orientational distributions of FM4-64, and the charge density of charged membranes also influences the orientational distribution, with higher charge opening the possibility of broader orientational distributions. The addition of Ca^{2+} ions in the solution leads to a change in the number of adsorbed probe molecules, which can be quantified for zwitterionic lipids. Because variations in the orientational distribution and surface number density due to different lipid compositions and ionic environment result in widely different SH responses, these factors must be accounted for when interpreting SH signals from voltage-sensitive probes.

SIGNIFICANCE Voltage-sensitive dyes used in second-harmonic imaging are used to uncover membrane potential. However, their response not only depends on voltage but also on the dye orientation and its surface number density. Using FM4-64 in giant unilamellar vesicles, we show that changes in lipid composition and in the ionic environment alter the orientational distribution and surface number density of the dye independently of the potential, leading to a different SH response. Experimental conditions that affect these two parameters must therefore be carefully considered to avoid misinterpreting the SH response and introducing errors on the obtained membrane potential.

INTRODUCTION

Voltage-sensitive dyes (VSDs) are fluorescent molecules used for the detection of electrical activity in living cells and tissues. Their use relies on the change in their optical properties in response to changes in membrane potential or applied potential.[1] VSDs have significantly impacted the field of electrophysiology by providing a noninvasive method to monitor neuronal[2–9] and cardiac activity[10–12] with high spatial and temporal resolution. Additionally, VSDs offer the advantage of capturing dynamic electrical events across large populations of cells or entire tissues. VSDs were originally used in fluorescence measurements[13,14] and were also applied in second harmonic (SH) microscopy, in which the surface sensitivity of the second harmonic generation (SHG) process was combined with the resonantly enhanced measurement of membrane potentials.[15–19] This has resulted in high-speed optical recordings

Submitted March 26, 2026, and accepted for publication July 6, 2026.

*Correspondence: arianna.marchioro@epfl.ch or sylvie.roke@epfl.ch

Editor: Carlos Baiz.

https://doi.org/10.1016/j.bpj.2026.07.006

Please cite this article in press as: Li et al., On the mechanism and voltage sensitivity of voltage-sensitive second harmonic probes: A case study of FM4-64, Biophysical Journal (2026), https://doi.org/10.1016/j.bpj.2026.07.006

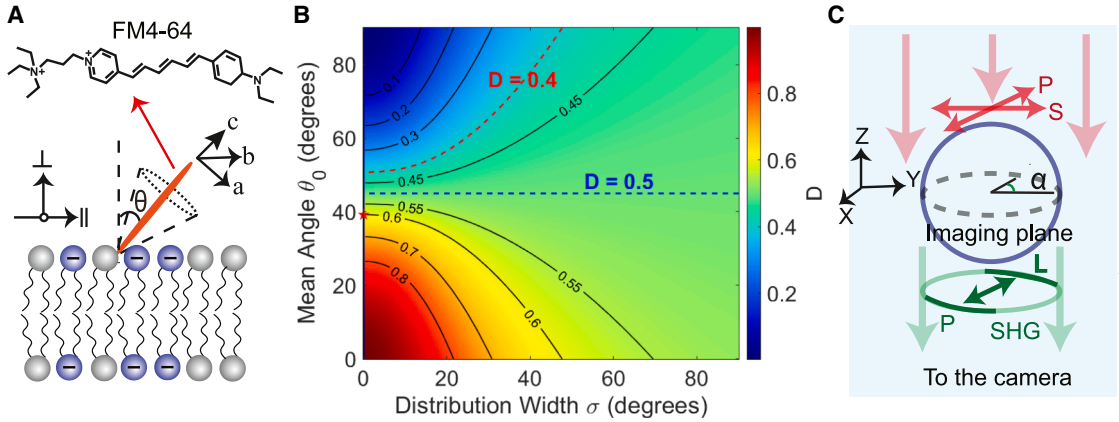

Figure 1. SH imaging of VSDs on GUV membranes and orientation parameter D. (A) Molecular structure of FM4-64 with an illustration of a cylindrical chromophore at a membrane interface, and the dashed cone schematically illustrates the orientational distribution. (B) Contour plot of the calculated orientation parameter D as a function of the mean tilt angle θ_0 and width σ of a Gaussian distribution. $D = 0.5$ (blue dashed line) physically indicates that the molecular orientational distribution may be very broad. The red star indicates the second-harmonic magic angle considering a one-dimensional molecular distribution as discussed in Simpson and Rowlen.[28] (C) Schematic diagram of the SH imaging of VSDs embedded in the outer leaflets of GUVs in solution. The red arrows represent the incident near-infrared (1,030 nm) illumination, and the green arrows represent the emitted (515 nm) SH light. L is the pixel-wise spatial position over the GUV equator. P and S indicate the polarization of the incoming/outgoing beams and are related to the X and Y directions of the laboratory frame. α defines the angle between the surface normal in the equatorial plane and the laser polarization direction.

of membrane potentials in various systems, including neurons and bacteria.[20–26] A typical example of a VSD is FM4-64,[27] an amphiphilic molecule with a chain of π-conjugated bonds whose structure is given in Figure 1A.

The voltage dependence of the resonant SH emission of VSDs inserted in lipid bilayers in relation to an applied or existing bias has been investigated in many studies.[20,25,29–32] The SH emission of VSDs under the influence of the external electric field ($\boldsymbol{E}(\omega)$) of exciting light is characterized by the macroscopic second-order polarization $\boldsymbol{P}^{(2)}$ (2ω). Two primary contributions to the SH emission arise at the interface of a lipid bilayer[27]: the first one is related to the surface second-order susceptibility $\chi_s^{(2)}$, originating from the orientational average along the surface normal of the second-order hyperpolarizability $\boldsymbol{\beta}^{(2)}$ of the VSDs inserted in the membrane. The second contribution is related to the effective third-order susceptibility $\chi^{(3)'}$. $\chi^{(3)'}$ accounts for interactions with a static electric field associated with an electrostatic potential difference $\Delta\Phi_0$. Therefore, $\chi^{(3)'}$ mediates the potential-modulated SH emission and is the macroscopic manifestation of the molecular third-order hyperpolarizability $\boldsymbol{\beta}^{(3)}$. Additionally, it may also give rise to SH emission due to electric-field-oriented VSDs in the bulk solution. In the case of VSDs, this second contribution is expected to be minor as the chromophores have a relatively low bulk concentration due to their amphiphilicity.[27,33] The induced nonlinear polarization at the second-harmonic frequency $\boldsymbol{P}^{(2)}$ (2ω) is therefore

$$\boldsymbol{P}^{(2)}(2\omega) = \varepsilon_0\left[\chi_s^{(2)}\boldsymbol{E}(\omega)\boldsymbol{E}(\omega) + \chi^{(3)'}\boldsymbol{E}(\omega)\boldsymbol{E}(\omega)\Delta\Phi_0\right] \quad (1)$$

The observed SH intensity is given by

$$I(2\omega) \backsim \left|\boldsymbol{P}^{(2)}(2\omega)\right|^2 \backsim \left\{\left|\chi_s^{(2)}\right|^2 + 2\chi_s^{(2)}\chi^{(3)'}\Delta\Phi_0 + \left|\chi^{(3)'}(\Delta\Phi_0)\right|^2\right\} I(\omega)^2 \quad (2)$$

Here, $\Delta\Phi_0$ represents the electrostatic potential difference across the membrane, which comprises both the intrinsic membrane potential and a contribution from an externally applied bias. Similar expressions as Equations 1 and 2 are used for nonresonant SH imaging of interfacial water at the glass/water interface,[34] free-standing lipid membranes/giant unilamellar vesicles (GUVs) in water,[35,36] and the membranes of living neurons in aqueous media.[37] The nonresonant response from interfacial water is ∼7 orders of magnitude smaller than the resonant response from VSDs and can therefore be neglected when investigating VSDs.[36]

Resonant SHG studies using VSDs demonstrated a linear response between the SH intensity and an external bias applied to the VSD-containing lipid bilayer.[31] Based on Equation 2, a linear response between the SH intensity and potential in the presence of a VSD indicates that the term $\left[2\chi_s^{(2)}\chi^{(3)'}\Delta\Phi_0\right]$ is dominant, and that $\chi_s^{(2)} > \chi^{(3)'}$. Therefore, any changes to the surface term $\chi_s^{(2)}$ (associated to $\boldsymbol{\beta}^{(2)}$) or, to a minor extent, to the effective third-order susceptibility term $\chi^{(3)'}$ (as discussed above, dominated by the $\boldsymbol{\beta}^{(3)}$ term) will modify the VSD response. So far, most studies employing VSDs have assumed that VSDs respond to changes in electrostatic potential difference by altering their electronic properties through field-induced

Please cite this article in press as: Li et al., On the mechanism and voltage sensitivity of voltage-sensitive second harmonic probes: A case study of FM4-64, Biophysical Journal (2026), https://doi.org/10.1016/j.bpj.2026.07.006

modulation of the molecule's electronic structure, thereby modulating the SH intensity by changes in both $\boldsymbol{\beta}^{(2)}$ and $\boldsymbol{\beta}^{(3)}$ terms (sometimes referred to collectively as the "effective" hyperpolarizability).[16,29,32] We will refer to this mechanism as the electro-optic response. However, other factors may contribute to the VSDs' response and change the dominant $\boldsymbol{\chi}_s^{(2)}$ term in the presence of a static electric field. Considering the molecular origin of SHG, the $\boldsymbol{\chi}_s^{(2)}$ response is[30]

$$\boldsymbol{\chi}_s^{(2)} = N_s \boldsymbol{\beta}^{(2)} \langle \cos^3 \theta \rangle , \quad (3)$$

where N_s is the surface number density of the VSD, θ is the tilt angle of the VSD with respect to the interface normal (Figure 1A), and $\langle \ldots \rangle$ denotes averaging over the orientational distribution function (ODF). Equation 3 therefore shows that to account for SH intensity changes, not only the changes in $\boldsymbol{\beta}^{(2)}$ via charge redistribution must be considered, but also variations in the surface number density of the VSDs and in their orientational distribution at the interface. Thus, attributing the VSDs' potential sensitivity solely to the effective hyperpolarizability of the dye under the influence of an electric field oversimplifies the underlying mechanism. Indeed, it has been shown by Pons et al. that the electric field alters the alignment of stilbazolium VSDs and consequently changes the SH response.[31] Later works have suggested that some VSDs show a noninstantaneous SH response that cannot be explained by invoking uniquely the electro-optic mechanism and must involve some conformational change.[38,39] Given this evidence, experimental data that consider structural changes in the membrane, a situation particularly relevant for living cells, are therefore needed.

Here, we systematically address the effect of the lipid composition and the presence of ions on the SH emission of FM4-64 inserted in GUVs. GUVs are vesicles composed of a lipid bilayer membrane that provide an ideal model system for well-controlled biophysical studies because of their cell-sized dimensions (in the tens of microns range), while also offering a protein-free and compositionally controllable lipid membrane environment. We first discuss how to extract the ODF of FM4-64 and how to use it to quantify membrane disorder. Then, we show how the different lipid compositions and the ionic environment in the aqueous phase (using Ca^{2+} as an example) act on the lipid membrane and FM4-64 ordering, directly influencing the ODF and surface number density of FM4-64. These variations in the orientational distribution and surface number density result in widely different SH intensities. As a result, any change in experimental conditions that may lead to variations in the ODF and surface number density should therefore be accounted for when converting SH signals to membrane potentials.

MATERIALS AND METHODS

Chemicals and cleaning procedures

1,2-diphytanoyl-sn-glycero-3-phosphocholine (DPhPC), 1,2-diphytanoyl-sn-glycero-3-phosphate (DPhPA), and 1,2-dioleoyl-sn-glycero-3-phosphocholine (DOPC) were purchased from Avanti Polar Lipids. $CaCl_2$ (99.999%), poly(vinyl alcohol) (PVA, Mw 146,000–186,000, >99%), bovine serum albumin (BSA, >99%), glucose, sucrose, and chloroform (>99.8%) were purchased from Sigma-Aldrich. N-(3-triethylammoniumpropyl)-4-(6-(4-(diethylamino)phenyl)hexatrienyl)pyridinium dibromide, commonly known as FM4-64, was purchased from Thermo Fisher. The molecular structure is shown in Figure 1. All chemicals were used as received. All aqueous solutions were made with ultrapure water (H_2O, Milli-Q UF plus, Millipore, electrical resistance of 18.2 MΩ · cm). All aqueous solutions were filtered with 0.1-μm Millex filters. The cover slips used in the imaging were pre-cleaned with piranha solution (1:3, 30% H_2O_2: 95%–97% H_2SO_4) and thoroughly rinsed with ultrapure water.

PVA-assisted GUV growth and transfer

GUVs were formed by gel-assisted growth with polyvinyl alcohol (PVA) following a method similar to the one of Weinberger et al.[40] Briefly, a 5% (w/w) solution of PVA in water was prepared and heated to 90°C in a water bath, and 50 μL of heated PVA was spread on a glass-bottom culture dish (FluoroDish, WPI) and dried for 1 h at 50°C. Charged lipids (PA) were mixed with DOPC or DPhPC in chloroform before film formation. The molar ratio of PA to PC lipids was varied according to the experimental condition (see results and discussion for specific ratios). After depositing the solution of lipids in chloroform on the dried PVA film, the sample was placed on a heat plate kept at 40°C for 30 min to 1 h to accelerate chloroform evaporation. The sample was then transferred to a vacuum desiccator or a chemical hood with continuous airflow and dried for a minimum of 3 h up to overnight. Samples were typically prepared 1 day before SH measurements. The GUVs were grown as follows: The growth chamber was filled with a solution composed of 50 mM sucrose to match the osmolarity of the observation solution. The growth chamber was observed using a light microscope to track the formation of vesicles. After the desired vesicle sizes were reached, typically in less than 20 min, the GUVs were transferred into the observation chamber using a pipette. GUVs were grown to a diameter around 40 μm as verified by white-light microscopy. All analyzed GUVs had diameters in the range of 30–50 μm. Due to the difference in density of the inside and outside solution, many GUVs were found to precipitate to the bottom of the observation chamber. The observation chamber was made using a cleaned cover slip, coated with BSA for passivation in order to prevent rupture of GUVs

Please cite this article in press as: Li et al., On the mechanism and voltage sensitivity of voltage-sensitive second harmonic probes: A case study of FM4-64, Biophysical Journal (2026), https://doi.org/10.1016/j.bpj.2026.07.006

that come into contact with the glass surface, and rinsed with ultrapure water. It was then placed inside the SH microscope and filled with an observation solution. For experiments without Ca^{2+}, the observation solution contained 50 mM glucose. For Ca^{2+} experiments, $CaCl_2$ was added to the observation chamber before GUV transfer, at a final concentration of 5 mM. The glucose concentration was adjusted to 35 mM in Ca^{2+} experiments to match the osmolarity of the solution inside the GUVs (50 mM sucrose). In all cases, FM4-64 was added from a 1 mM stock solution to the observation chamber containing GUVs, achieving a final concentration of 2 μM.

Second-harmonic imaging of GUVs

The multiphoton microscope used in this work builds on the foundations of other imaging systems developed in our laboratory and is optimized for the highest possible efficiency of label-free SH imaging of GUVs.[36] Figure S1 shows the schematic diagram of the SH microscope. The microscope is powered by a femtosecond laser source (Femtolux 3, 1,030 nm, 1 MHz, 220 fs). The combination of a lens (f = 25 cm, N-BK7 uncoated Plano-Convex Lenses, Thorlabs) and a 60× water immersion objective lens (Olympus LUMPFLN 60XW, NA 1.0) allows the laser beam to excite an area of around 90 μm on a sample plane at normal incidence angle. The excitation power at the sample was set to 20 mW (corresponding to a fluence of 0.314 mJ/cm^2), measured after the objective. The SH light is collected in the forward direction with a 60× objective lens (Olympus LUMFLN 60XW, NA 1.1). A 750-nm short-pass filter (FESH0750, Thorlabs) and a 515-nm band-pass filter (FL514.5–10, Thorlabs) are used in the detection path to remove the fundamental beam. For polarization control, a half-wave plate for the fundamental beam and a combination of a half-wave plate and a Glan-Taylor prism for the detected light are used. The collected SH light is imaged into an electronically amplified intensified CCD camera (EM-iCCD, PiMax-4, Princeton Instruments) with an f = 18 cm lens (TTL 180A, Thorlabs). The camera was gated at a frequency corresponding to the repetition rate of the laser. SH images were collected with the gain set to 100. The recorded images had an equivalent pixel size on the sample of 400 nm. The GUV's diameter was approximately 40 μm. The nonlinear axial detection depth was 800 nm. The membrane curvature angle over an 800-nm length was < 3°, making a planar approximation of the interface accurate. For white-light imaging, the sample is illuminated from the top using a white-light source, and the linear scattered light is detected in the forward direction with the same objective lens. The main body of the microscope is built on top of a Rapid Automated Modular Microscope frame (RAMM system, ASI imaging). Translation of the sample is performed using an XYZ translation stage (PZ-2000FT, ASIimaging). X and Y positioning is performed using motors with linear encoders, while Z positioning is performed using a piezo stack (300-μm travel range).

Theoretical background

Before experimentally investigating how number density and orientational distribution impact the estimated electrostatic potential difference derived from measuring SH intensity, we review how the ODF enters the susceptibility/intensity expression and what can be experimentally deduced from measuring the SH intensity in different polarization combinations. The second-order susceptibility of a surface or interface arises from averaging the molecular hyperpolarizability ($\boldsymbol{\beta}^{(2)}$) elements of its constituent molecules (Equation 3). Since $\boldsymbol{\beta}^{(2)}$ is also direction sensitive, molecular contributions must be represented considering each molecular orientation with respect to the surface. Based on a known molecular symmetry and an ODF (denoted as function f) that in its complete form involves three Euler angles, each of which may have their own distribution, relationships between $\boldsymbol{\chi}_s^{(2)}$ and $\boldsymbol{\beta}^{(2)}$ can be calculated.[41,42] For an in-plane nonchiral isotropic surface, only the tilt angle θ of the molecular axis with respect to the surface normal is needed (see Figure 1A, and the ODF becomes $f(\theta)$). For this case, $\boldsymbol{\chi}_s^{(2)}$ depends on the molecular density N_s, θ, and $\boldsymbol{\beta}^{(2)}$[41–43]:

$$\begin{pmatrix} \chi_{s1}^{(2)} \\ \chi_{s2}^{(2)} \\ \chi_{s3}^{(2)} \\ \chi_{s4}^{(2)} \end{pmatrix} = \frac{N_s\langle\cos\theta\rangle}{2} \begin{pmatrix} 5D-3 & 0 & 0 & 0 \\ 1-D & 2 & 0 & 0 \\ 1-D & 0 & 2 & 0 \\ 1-D & 0 & 0 & 2 \end{pmatrix} \begin{pmatrix} \beta_1^{(2)} \\ \beta_2^{(2)} \\ \beta_3^{(2)} \\ \beta_4^{(2)} \end{pmatrix}$$

and

$$D = \frac{\langle cos^3\,\theta\rangle}{\langle\cos\theta\rangle} \tag{4}$$

with $\chi_{s1}^{(2)} = \chi_{\perp\perp\perp}^{(2)} - \chi_{\|\|\perp}^{(2)} - \chi_{\|\perp\|}^{(2)} - \chi_{\perp\|\|}^{(2)}$, $\chi_{s2}^{(2)} = \chi_{\|\|\perp}^{(2)}$, $\chi_{s3}^{(2)} = \chi_{\|\perp\|}^{(2)}$, and $\chi_{s4}^{(2)} = \chi_{\perp\|\|}^{(2)}$; and $\beta_1^{(2)} = \beta_{ccc}^{(2)} - \beta_2^{(2)} - \beta_3^{(2)} - \beta_4^{(2)}$, $\beta_2^{(2)} = \frac{(\beta_{aac}^{(2)}+\beta_{bbc}^{(2)})}{2}$, $\beta_3^{(2)} = \frac{(\beta_{aca}^{(2)}+\beta_{bcb}^{(2)})}{2}$, and $\beta_4^{(2)} = \frac{(\beta_{caa}^{(2)}+\beta_{cbb}^{(2)})}{2}$, using (a,b,c) as the right-handed coordinate system of the molecule (Figure 1A). N_s is the surface number density of molecules. $\langle cos\,\theta\rangle$ denotes the average cosine of the tilt angle θ between the c axis of the molecule and the surface normal (the $\perp$ direction).[44] For a rod-like chromophore such as FM4-64, the molecular second-order and third-order hyperpolarizability tensors are approximated by a single tensor element, $\beta_{ccc}^{(2)}$ and $\beta_{cccc}^{(3)}$ along its symmetry axis.[45] The orientational parameter D defined in Equation 4 can be determined from the SH intensity recorded at different polarization combinations, as will be described explicitly below.

Please cite this article in press as: Li et al., On the mechanism and voltage sensitivity of voltage-sensitive second harmonic probes: A case study of FM4-64, Biophysical Journal (2026), https://doi.org/10.1016/j.bpj.2026.07.006

An interfacial orientational distribution can have any configuration between completely aligned along the surface normal (that is, all molecules have precisely the same orientation perpendicular to the surface) to a completely random distribution (that is, each value of θ appears equally often). For the first scenario $\langle cos\,\theta\rangle = 1$ and $D = 1$, so that Equation 3 simplifies to $\chi_{si}^{(2)} = N_s\beta_i^{(2)}$, where i denotes one of the indices of the matrix in Equation 4. For the second scenario, we have $\langle cos\,\theta\rangle = 0$ and $D = 0$, so that Equation 3 simplifies to $\chi_{si}^{(2)} = 0$. The actual molecular orientation distribution at an interface will be in between those extremes. Equation 4 cannot be solved explicitly and without assumptions from the available independent polarization combinations that can be measured in an SH or sum frequency generation experiment from an isotropic interface. Therefore, a number of studies have aimed to simplify the involved relations (reviewed in Wang et al.[46]). Assuming that only the polar angle is relevant reduces the expressions connecting $\boldsymbol{\chi}_s^{(2)}$ to $\boldsymbol{\beta}^{(2)}$ to a simpler expression,[43,47] and this would be a reasonable assumption for a cylindrical chromophore, such as FM4-64 as used in this study. If the interfacial molecules are highly ordered, ODFs can be modeled as δ-functions or Gaussian distributions that have widths $<\sim 15°$,[46,48] in which case an average tilt angle and tilt angle distribution can be determined from comparing intensities measured in different polarization combinations. However, when the tilt angle distribution is broad, the ODF is better described by a cosine Legendre polynomial series, and a single tilt angle or range of tilt angles cannot be retrieved from the data.[28,49] If one performs SHG or SFG experiments to obtain the molecular tilt angle distribution from an interface containing a broad molecular distribution and analyzes the data under the assumption that all molecules have the same tilt angle (i.e., taking $f(\theta) = \frac{\delta(\theta-\theta_0)}{\sin(\theta)}$), one incorrectly arrives at the conclusion that $\theta_0 \sim 39.2°$. This θ_0 is referred to as the "magic angle."

Alternatively, one can think of the distribution as undetermined since an SH measurement cannot be used to make any statements about the width. To illustrate this and the significance of it for understanding molecular distributions based on SHG measurements, we next assume that the ODF ($f(\theta)$) is a Gaussian function in 3 dimensions (illustrated by the cone in Figure 1A). For any quantity $g(\theta)$, the ensemble average over molecular orientations in an azimuthally isotropic system, considering a Gaussian distribution for the probability distribution of molecular orientations, can be written as $\langle g(\theta)\rangle = \frac{\int_0^{\frac{\pi}{2}} g(\theta) e\left(-\frac{(\theta-\theta_0)^2}{2\sigma^2}\right)\sin\theta d\theta}{\int_0^{\frac{\pi}{2}} e\left(-\frac{(\theta-\theta_0)^2}{2\sigma^2}\right)\sin\theta d\theta}$. Substituting this expression in Equation 4, the parameter D becomes

$$D = \frac{\int_0^{\frac{\pi}{2}} \cos^3\theta \exp\left(-\frac{(\theta-\theta_0)^2}{2\sigma^2}\right)\sin\theta d\theta}{\int_0^{\frac{\pi}{2}} \cos\theta \exp\left(-\frac{(\theta-\theta_0)^2}{2\sigma^2}\right)\sin\theta d\theta} \quad (5)$$

Figure 1B shows a contour plot of the parameter D calculated as a function of the mean tilt angle of the distribution (θ_0, y axis) and the width (σ, x axis). Smaller values of σ indicate a narrower distribution (strong molecular alignment), while larger values of σ are representative of a large distribution width (weak alignment, or a broad molecular distribution).

The plot in Figure 1B illustrates that a specific D value (indicated by the black contour lines) can be obtained with a variety of different combinations of the parameters θ_0 and σ. The intersections of the contour lines with the σ axis determine the maximum plausible degree of disorder of the system. For example, the line at $D = 0.1$ shows that a measurement that gives a value of $D = 0.1$ can originate from multiple distributions, having either a δ-function distribution with an angle of $\sim 70°$ or even larger tilt angles with progressively broader distributions. $D = 0.4$ shows a similar trend but permitting even larger distribution width. $D = 0.5$ is a horizontal line, indicating that any value of σ between 0° and 90° is accessible, and that the corresponding distribution mean angle is $\theta_0 = 45°$. Therefore, D values close to 0.5 indicate the possible presence of a broad molecular distribution, as they account for the possibility to have distribution width with $\sigma > 70°$. This result is similar to what was obtained previously for a 1-dimensional distribution of θ_o values, which results in $D = 0.6$ and $\theta_0 = 39.2°$ (assuming a δ-function as ODF).[28] Figure 1B also shows that values of $D > 0.6$ indicate that the molecules are, on average, oriented closer to the surface normal (more upright, with the mean tilt angle < 45°). Conversely, values of $D < 0.4$ indicate that molecules are preferentially oriented closer to the surface plane (lying down, with the mean tilt angle > 45°).

It is important to note that D alone does not uniquely determine the orientational distribution, but it rather defines the range of possible mean tilt angles and distribution widths (Figure 1B). Within the range defined for a specific D value, we assume that all orientational distributions within the allowed range are equally probable. This assumption does not affect our study: indeed, in what follows, we do not attempt to derive an averaged orientational angle of chromophores from SH images but rather derive D values and use them to infer if orientations have changed, and how this might reflect membrane structural changes. In our experiments on GUVs, SH photons are emitted in the polarization directions S and P, perpendicular and parallel to the imaging plane (plane of incidence). Two independent polarization combinations are recorded, I_{PPP} with all beams identically polarized parallel to the imaging plane and I_{PSS}

Please cite this article in press as: Li et al., On the mechanism and voltage sensitivity of voltage-sensitive second harmonic probes: A case study of FM4-64, Biophysical Journal (2026), https://doi.org/10.1016/j.bpj.2026.07.006

with the SH beam polarized parallel to the imaging plane and the incoming beams polarized perpendicular to the SH beam. With α the angle between the surface normal in the equatorial plane and P direction, the SH intensity is as follows:

$$I_{PPP} = C\left(1+\frac{\beta^{(3)}_{CCCC}\langle\cos\theta\rangle\Phi_{0,1}}{\beta^{(2)}_{CCC}}\right)^2\left(\langle\cos^3\theta\rangle\cos^3\alpha + \frac{3}{2}\langle\cos\theta - \cos^3\theta\rangle\cos\alpha\sin^2\alpha\right)^2 \quad (6)$$

$$I_{PSS} = C\left(1+\frac{\beta^{(3)}_{CCCC}\langle\cos\theta\rangle\Phi_{0,1}}{\beta^{(2)}_{CCC}}\right)^2\left(\langle\cos^3\theta\rangle\cos\alpha\sin^2\alpha + \frac{1}{2}\langle\cos\theta - \cos^3\theta\rangle\cos\alpha\left(1 - 3\sin^2\alpha\right)\right)^2$$

The detailed derivation of these equations can be found in the supplemental information S3. The orientation distribution parameter D can be derived from the ratio[31]:

$$\sqrt{\frac{I_{PPP}}{I_{PSS}}} \sim \left|\frac{D\cos^3\alpha + \frac{3}{2}(1-D)\cos\alpha\sin^2\alpha}{D\sin^2\alpha\cos\alpha + \frac{1}{2}(1-D)\cos\alpha\left(1-3\sin^2\alpha\right)}\right| \quad (7)$$

Note that there is no dependence on an electrostatic potential difference in Equation 7 as it cancels out if we take the ratio of I_{PPP}/I_{SSS}. We can therefore use the parameter D to assess whether the ODF changes, and by how much it changes for different lipid compositions and chemical environments in GUVs.

RESULTS AND DISCUSSION

Effect of lipid ordering in neutral membranes

We next investigate if the ODF of FM4-64 depends on lipid structure, as characterized by the parameter D. Single-lipid GUVs prepared with neutral lipids, DOPC and DPhPC, were employed to investigate the effect of membrane ordering on the ODF. In the case of neutral lipids and in the absence of an external bias, $\Delta\Phi_0$ is on average equal to zero, and the SH intensity is therefore directly related to the magnitude of $\chi^{(2)}_s$ as shown in Equation 2. DOPC is an unsaturated lipid, while DPhPC is a branched saturated lipid. This difference provides a useful framework for investigating how the ODF of the dye changes in distinct lipid environments.

Equation 7 shows that two measurements, in the PPP and PSS polarization combinations, need to be performed to extract D. We therefore conducted polarization measurements using the PPP and PSS polarization combinations on both DOPC and DPhPC GUVs. Figures 2A and 2B show the SH images of a DOPC GUV and a DPhPC GUV, respectively, in a glucose/sucrose solution (outside/inside) stained with FM4-64 on the outer leaflet for both PPP and PSS polarization combinations. The concentration of FM4-64 was set to 2 μM in the outside solution. The SH intensity in the PSS polarization combination was magnified three times for better visualization. The data in Figures 2A and 2B can then be used to determine the orientation parameter D. We focus on the regions along the GUV equator where the signal-to-noise ratio is sufficiently high in both polarization combinations, schematically denoted as L in Figures 1C and 2A. To do so, we use the intensity profiles along the GUV equator between 55° and 125°, starting from the right end of the GUV equator as shown in Figure 2A. In this region, both the numerator and denominator are positive in Equation 7 (the term 1-3sin$^2\alpha$ is positive).

The spatial variation of D as a function of L was obtained from DOPC and DPhPC GUVs, and two representative GUVs for each lipid type are shown in Figure 2C. A profile length of 50 pixels corresponds to a physical distance of ∼20 μm along the GUV equator. The GUVs composed of DOPC (blue triangles) show D values higher than for the GUVs made of DPhPC (red squares). Furthermore, the spatial fluctuations of D point to a nonuniform orientation distribution of FM4-64 across the membrane surface. The lower values of D occasionally observed in DPhPC GUVs (e.g., Figure 2C) are not present in all vesicles (see Figure S4) and may arise from local membrane defects or a small fraction of dye molecules with different insertion geometry. This spatial heterogeneity contributes to the width of the D value distribution but does not affect the comparison between averaged values of both lipids shown in Figure 2D.

To better quantify the difference between DOPC and DPhPC GUVs, histograms of D values extracted from 10 different GUVs for each lipid are plotted in Figure 2D. The distribution of D values is fitted with a Gaussian distribution (indicated by the solid line). Specifically, the D values of the DOPC GUVs consistently fall in a distribution centered at $\overline{D} = 0.5$, $\overline{D}$ being the mean value of the Gaussian distribution. The D values observed for DOPC are higher than those observed for DPhPC GUVs ($\overline{D} = 0.42$). From the distribution histograms in Figure 2D, we also extracted the full width at half maximum (FWHM), an intuitive parameter indicating the degree of fluctuation. For DOPC GUVs, the FWHM is around 0.08, corresponding to a fluctuation percentage of 16%. For DPhPC GUVs, the FWHM is 0.07, which is a similar value as obtained for DOPC. Based on the results of Figure 1B, the D values obtained for FM4-64 in different GUVs give some information about the maximum plausible degree of disorder. With $\overline{D} = 0.42$, FM4-64 on DPhPC spans a range of orientation distribution widths from 0° up to 54°, while FM4-64 on DOPC displays $\overline{D} = 0.5$, indicating that distribution widths spanning the full range from 0° to 90° are possible, including very broad

Please cite this article in press as: Li et al., On the mechanism and voltage sensitivity of voltage-sensitive second harmonic probes: A case study of FM4-64, Biophysical Journal (2026), https://doi.org/10.1016/j.bpj.2026.07.006

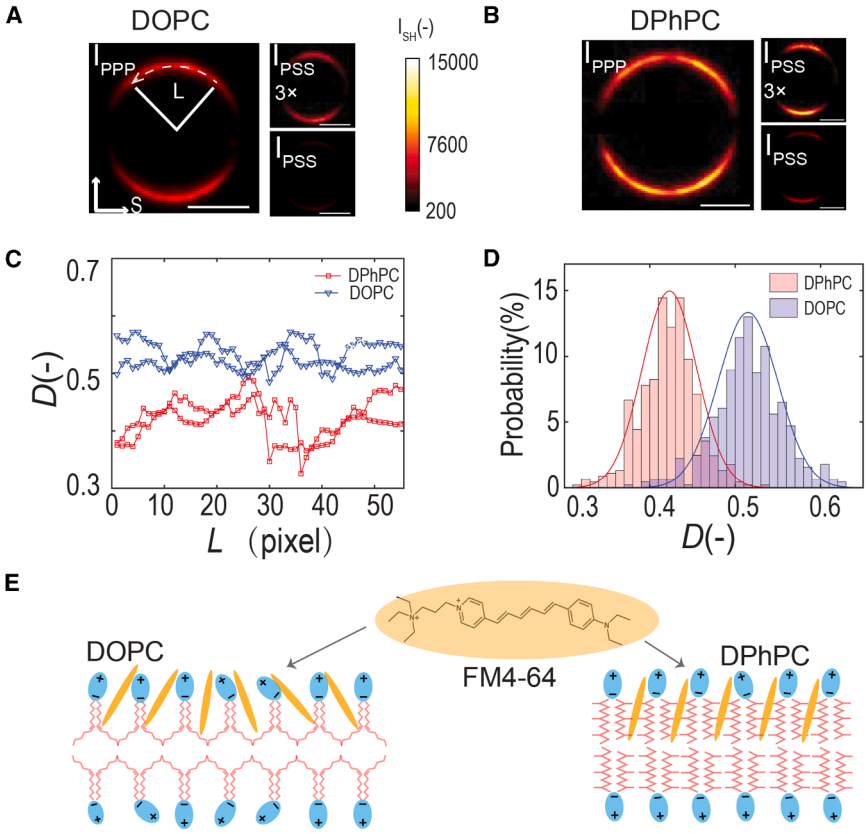

Figure 2. Orientation distribution of FM4-64 on GUV membranes with different zwitterionic lipid compositions. (A and B) SH images of DOPC and DPhPC GUVs, respectively, acquired using the PPP (left) and PSS (right) polarization configurations. The concentration of FM4-64 was set to 2 μM in the outer aqueous solution to ensure the dye could insert in the outer leaflet of the GUV membrane. The PSS SH intensity is shown multiplied 3 times (top image) and as recorded (bottom one). Scale bar: 20 μm. (C) Spatial distribution of D for FM4-64 as a function of L (the pixel-wise spatial position over the GUV equator) for different GUVs prepared with DOPC and DPhPC. Each pixel (symbol) corresponds to 400 nm in physical length, and each line corresponds to a different GUV. (D) Histogram showing the overall distribution of D values for 10 DOPC and 10 DPhPC GUVs, highlighting distinct differences between the two lipid compositions. The solid line represents a Gaussian fit to the histogram. (E) Schematic illustration of the influence of lipid ordering on the orientation of FM4-64. GUVs made with DOPC lipids exhibit D values centered at 0.5 ($\overline{D} = 0.5$), suggesting a broader orientation distribution due to lower membrane ordering is possible.

distributions with widths exceeding 70°. This difference likely reflects the more ordered structure of the DPhPC bilayers, as schematically illustrated in Figure 2E, and would be consistent with the expectation that saturated lipids exhibit a higher packing order than unsaturated lipids such as DOPC, as also demonstrated with previous studies using X-ray diffraction or NMR.[50–53] Nonetheless, it is interesting to note that the branched acyl chains do confer special properties to DPhPC. The area per lipid of DPhPC is high (80.5 $Å^2$ at 30°C)[54] relative to other saturated lipids such as DPPC or DMPC (values range between 47.9 $Å^2$ at 20°C to 71.2 $Å^2$ at 50°C),[55] and a high area per lipid is commonly taken as an indicator of a poorly packed structure. Furthermore, the melting temperature of DPhPC is very low (<−120°C),[56] which is also a typical characteristic of lipids forming more disordered bilayers. Despite these factors, DPhPC has been found to form stable bilayer membranes with low ion leakage[57] and to have an order parameter close to other phospholipids forming liquid crystalline phases.[56] In such liquid crystalline phases, a certain degree of fluidity is allowed, while still retaining structural order. Our SH results therefore further support the formation of structurally ordered bilayer membranes with DPhPC, at least in comparison with DOPC.

Fluorophores inserted in membranes have been shown to relocate to the inner leaflet over time[58] and flip-flop of a styryl dye such as Di-6-ASPBS has been shown to occur.[59] Flip-flop of an SH-emitting molecule reduces the SH intensity as a result of the increasing centrosymmetry, and Moreaux et al.[59] report a decay of the SH signal intensity to half of the initial value after 1 h. In our experiments, a single GUV measurement required only a few minutes, during which we observed no obvious decay in SH intensity. Over such a short interval, flip-flop is therefore considered to be negligible.

Thus, VSDs embedded in single-lipid GUVs made of two different zwitterionic lipid membranes display different orientational distributions, which indicates that SH intensity changes of VSDs are not solely due to electro-optical effects.

Effect of lipid ordering in charged membranes

Having tested the effect of different lipid composition on the membrane packing order, we next investigate how varying the proportion of charged lipids (DPhPA, containing the phosphatidic acid [PA] charged headgroup) affects the ODF of the membrane-associated FM4-64, due to lipid ordering being influenced by electrostatic interactions. Contrarily to the neutral membranes investigated above, the presence of charged lipids may affect the electrostatic term in Equation 2. Each leaflet of the lipid membrane can be characterized by its surface potential, defined as the potential difference between the surface and the bulk solution. In

Please cite this article in press as: Li et al., On the mechanism and voltage sensitivity of voltage-sensitive second harmonic probes: A case study of FM4-64, Biophysical Journal (2026), https://doi.org/10.1016/j.bpj.2026.07.006

the following, $\Phi_{0,1}$ and $\Phi_{0,2}$ denote the surface potentials of the outer and inner leaflets. The transmembrane potential difference is then given by the difference between these two terms: $\Delta\Phi_0 = \Phi_{0,1}$-$\Phi_{0,2}$. If the charged lipids distribute homogeneously between the inner and outer leaflet ($\Phi_{0,1} = \Phi_{0,2}$), no transmembrane potential difference is present in the system. However, the surface potential difference between each individual leaflet and its surrounding solution can still be sensed by a voltage-sensitive probe. As discussed above, FM4-64 inserts in the outer leaflet of the GUV, and flip-flop to the inner leaflet is not observed. The chromophore thus reports on the surface potential of the outer leaflet ($\Phi_{0,1}$).

While the effect of an electrostatic potential difference on the VSD SH emission is expected through modulation of the electro-optic response, the influence of charged lipids on the ODF of the VSD has not been considered in other studies. With the method developed above to calculate the orientation parameter D, we can selectively separate the effect of charged lipids on the ODF from their effect on the electro-optic response. Figures 3A–3C show SH images of GUVs made with branched lipids with different PA:PC ratios, 50:50, 30:70, and 0:100, respectively, acquired using the PPP polarization configuration. Figure 3D shows the histogram of D values for DPhPC/PA (50:50) and DPhPC/PA (70:30) compared with the pure DPhPC sample (10 GUVs of each composition were measured). The mean D value for DPhPC/PA (50:50) ($\overline{D} = 0.51$) is higher than that of neutral DPhPC GUVs ($\overline{D} = 0.42$). We interpret this increase as suggesting the possibility of a broader orientational distribution of FM4-64 on the DPhPC/PA surface, resulting from reduced lipid ordering. This increased disorder is attributed to electrostatic repulsion between negatively charged PA headgroups, as illustrated in Figure 3E, which leads to a more disordered membrane environment and thus a wider orientational distribution of the dye.

To further test this hypothesis, we examine GUVs with a lower charge density (DPhPC/PA 70:30), as shown in Figure 3D. The mean D value of the GUVs with DPhPC/PA (70:30) ($\overline{D} = 0.46$) is intermediate between the case of neutral lipids and the highly charged ones, which is consistent with our interpretation. These findings indicate that the ODF is directly affected by changes in the lipid bilayer structure due to variations in the charge density within the membrane.

Ion effects in charged membranes

In the following parts, we investigate the effects of a representative divalent cation, Ca^{2+}, on the SH emission of FM4-64 embedded in the membrane environment. We first use negatively charged GUVs composed of DPhPC/PA (50:50). Figures 4A and 4B show SH images of GUVs made of DPhPC:PA (50:50) with and without Ca^{2+} in the external solution, respectively. With the presence of 5 mM Ca^{2+} ($CaCl_2$) in the external solution, the SH intensity decreases by two orders of magnitude in this image. Figure 4C presents the average SH intensity from 8 GUVs in

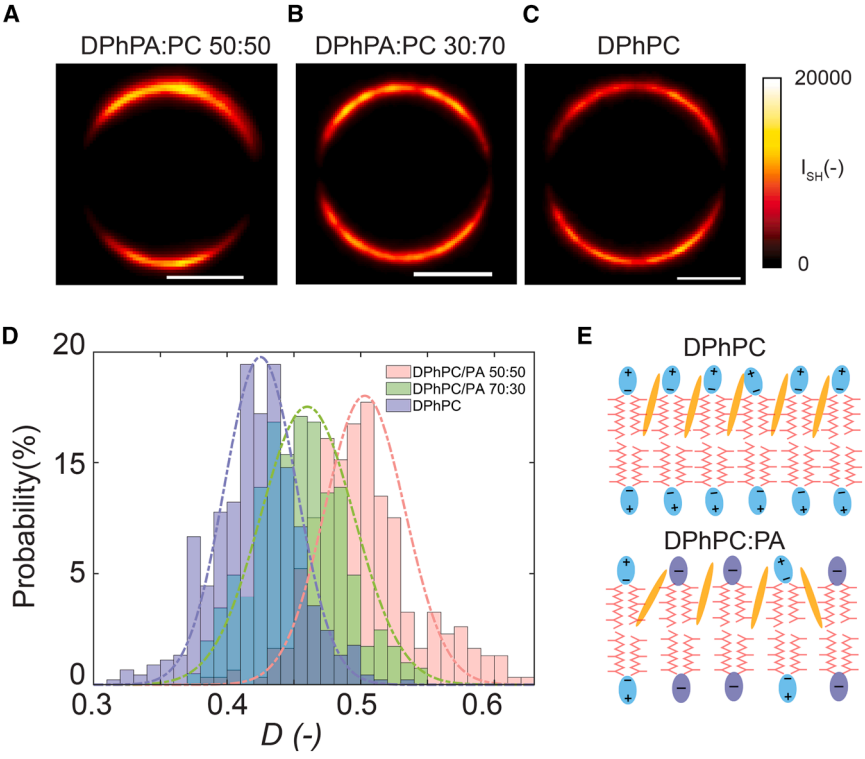

Figure 3. Effect of charge on lipid membrane organization and FM4-64 orientation. (A–C) SH images of GUVs made of branched lipids with different PA:PC headgroup ratios, 50:50, 30:70, 0:100, respectively, acquired using the PPP polarization configuration. Scale bar: 20 μm. The concentration of FM4-64 was set to 2 μM in the outer aqueous solution. (D) Variation in D values on membranes with a different percentage of negatively charged PA lipids. 10 GUVs were measured for each lipid composition. (E) Schematic illustration of the different orientational distribution of FM4-64 with increasing charge.

Please cite this article in press as: Li et al., On the mechanism and voltage sensitivity of voltage-sensitive second harmonic probes: A case study of FM4-64, Biophysical Journal (2026), https://doi.org/10.1016/j.bpj.2026.07.006

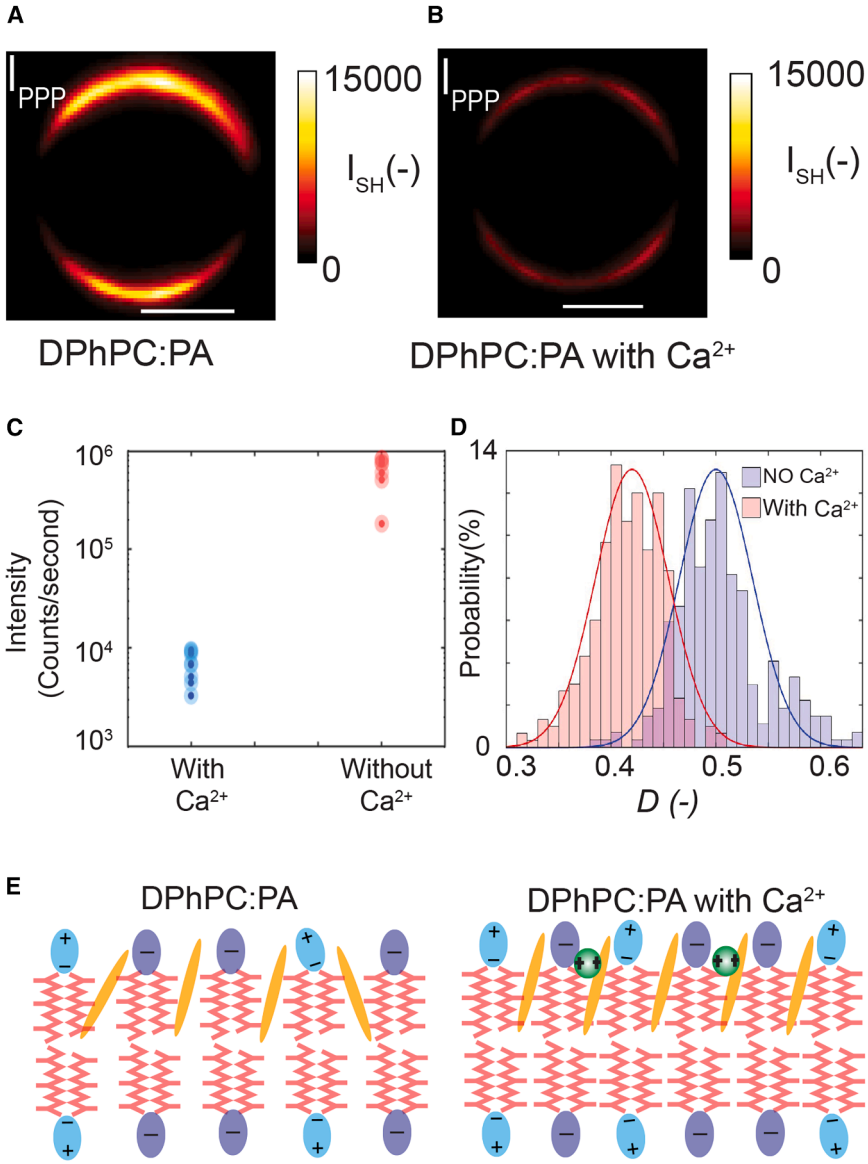

Figure 4. The effect of Ca^{2+} on the SH emission of FM4-64 inserted in charged membranes. (A and B) SH images of GUVs made of DPhPC:PA (50:50) with and without Ca^{2+} in the external solution. The concentration of Ca^{2+} is 5 mM. A decrease in the SH intensity can be observed after Ca^{2+} addition. Scale bar: 20 μm. (C) Averaged SH intensity (counts/second) for a series of 8 different DPhPC:PA GUVs with and without Ca^{2+} in the outside solution (each point represents a single GUV). (D) Corresponding D parameter showing a significant change in the presence of Ca^{2+} (obtained for 8 GUVs in each case). (E) Schematic representation of the effect of Ca^{2+} ions on DPhPC:PA lipid ordering and FM4-64 membrane association.

presence and absence of Ca^{2+}. The SH intensity differs by two orders of magnitude between the two conditions. These results highlight a strong ion-induced modulation of the dye's nonlinear optical response.

Here, several effects are expected to modulate the SH emission of the FM4-64 upon Ca^{2+} addition: (1) the binding of Ca^{2+} to the negatively charged PA headgroups neutralizes the membrane surface charge and reduces the surface potential $\Phi_{0,1}$, therefore reducing the FM4-64 emission intensity (Equation 2); (2) FM4-64 carries a positive charge and preferentially associates with negatively charged membranes; thus, Ca^{2+}-induced surface charge neutralization could result in a reduced dye incorporation (lower N_s) and a corresponding decrease in the total SH intensity; (3) the neutralization of the electrostatic repulsion between negatively charged PA headgroups may lead to a different ODF of FM4-64.

According to Li et al.,[60] the average surface potential of DPhPC/PA (50:50) GUVs is approximately 250 mV. As shown in Figure S2, a surface potential change of 100 mV results in a 4.4% variation in the SH intensity. Therefore, a complete depolarization of the membrane potential can account for at most an ∼11% reduction in the SH signal (effect 1). Consequently, the remaining ∼88% decrease in SH emission must originate from changes in the molecular number density at the interface (effect 2) and/or modifications of the ODF of the chromophores (effect 3). In the case of charged membranes, it is not possible to quantitatively estimate the surface number density of FM4-64 from the SH images (quantitative estimation of N_s is however possible for neutral membranes, as described below). As a result, for charged GUVs, it is not possible to unambiguously determine whether the observed SHG reduction is

Please cite this article in press as: Li et al., On the mechanism and voltage sensitivity of voltage-sensitive second harmonic probes: A case study of FM4-64, Biophysical Journal (2026), https://doi.org/10.1016/j.bpj.2026.07.006

dominated by a decrease in the VSD surface number density or by changes in molecular orientation. Nevertheless, the D parameter can be determined independently and serves as a sensitive indicator of changes in the ODF.

We extract the orientation parameter D from the SH images of 8 GUVs for each composition (with and without Ca^{2+}) and plot the resulting histograms in Figure 4D. Figure 4D shows that the D values decrease when Ca^{2+} is added to the solution ($\overline{D} = 0.42$), compared with conditions without Ca^{2+} ($\overline{D} = 0.51$). Therefore, the orientation distribution of FM4-64 becomes narrower in the presence of Ca^{2+}. The narrowing of the distribution can be attributed to Ca^{2+} binding to the negatively charged phosphate groups and neutralizing the membrane charges, which promotes lipid ordering within the membrane and consequently decreases the orientational distribution parameter D, as depicted in Figure 4E. These results are consistent with the ones of the charged lipid membrane with different proportions of charged lipids, shown in Figure 3, where a decreasing membrane charge also promotes lipid ordering.

Note that Ca^{2+} could potentially alter the presence/structure of FM4-64 in the outer leaflet. For instance, Ca^{2+} binding to negatively charged headgroups might reduce electrostatic repulsion and promote flip-flop. Here as well, we did not observe a decrease in the total SH intensity within the measurement time frame (minutes). The absence of such a decrease is inconsistent with significant signal cancellation from inner-leaflet dye, suggesting that flip-flop is negligible on our timescale.

These findings highlight the critical role of multiple factors, and not only of an electrostatic potential difference, in interpreting SH signals from VSDs, underscoring the need to account for ODF effects and FM4-64 surface number density when analyzing SH images in complex membrane environments. A recent study comparing electrical recordings with voltage measurements from SH FM4-64 and SH water imaging shows that the latter can be an alternative method to record electrostatic potential differences.[61]

Ion effects on neutral membranes

To further distinguish between the effects of ions on the FM4-64 surface number density N_s and on its ODF from their effect on the surface potential $\Phi_{0,1}$, we employed electrically neutral DPhPC GUVs, where $\Phi_{0,1} = 0$, on average. Figure 5A shows SH images of a DPhPC GUV with and without Ca^{2+} ions in the solution. The comparison of the two images reveals a decrease in SH intensity upon the addition of 5 mM $CaCl_2$. To confirm that the surface potential remains unchanged upon addition of ions, we measured the ζ-potential of neutral liposomes (400 nm diameter) composed of the same lipids with and without Ca^{2+}. The ζ-potential remained between −1 and +5 mV, suggesting that no major change in surface potential occurs after addition of $CaCl_2$ (see supplemental information S5). This result allows us to rule out the effect of surface potential and, by extension, dismiss any significant influence of Ca^{2+} on the electro-optic response of FM4-64 (effect 1 discussed above). The remaining two factors potentially responsible for the observed SH intensity change are the surface number density of the dye and the ODF as discussed above (effects 2 and 3). For a neutral membrane, the SH intensity is directly related to $\chi_s^{(2)}$ and therefore $\beta^{(2)}$ (Equations 2 and 3). Knowing $\beta^{(2)}$ of the FM4-64, one can therefore estimate N_s (detailed calculation is in supplemental information S6). The orientation distribution parameter D and N_s are plotted in Figures 5B and 5C, respectively. In this case, the analysis of D in Figure 5B shows no appreciable difference between conditions with and without Ca^{2+}. Conversely, quantitative calculations of N_s on the membrane surface in Figure 5C show that the calculated N_s decreased by one order of magnitude, from 0.01 molecules/nm^2 to 0.001 molecules/nm^2, upon the addition of Ca^{2+}. To enable the comparison with N_s, the bulk dye concentration of 2 μM can be converted to an equivalent surface number density by assuming a hypothetical 3-nm-thick layer, yielding 3.6×10^{-6} molecules/nm^2. This calculated value can be considered as the upper limit in an unlikely case where no molecule added to the bulk solution would absorb at the surface, and therefore one can realistically consider even lower values. The estimation of the equivalent surface number density for the bulk dye being orders of magnitude lower than the molecular surface density N_s calculated for the membrane, it indicates that FM4-64 is an amphiphilic dye that preferentially partitions into lipid membranes.[33]

At the molecular level, the results from Figures 5B and 5C can be understood as follows: in DPhPC bilayers, which are already structurally compact, Ca^{2+} does not significantly enhance the order of the membrane and therefore does not modify the D values. In contrast, the observed reduction of N_s can be attributed to Ca^{2+} ions binding with the negative part of the PC headgroup, which leads to exclusion of the positively charged FM4-64 molecules from the membrane surface, as illustrated in Figure 5D. This experiment therefore provides strong evidence that the VSD surface number density is a crucial factor influencing the SH signal intensity and should be considered as one of the key mechanisms modulating the VSD SH response.

To assess the general applicability of these findings, we extended our investigation to GUVs composed of DOPC, as shown in Figure 5E. In contrast to the DPhPC system, the presence of Ca^{2+} does affect the orientation distribution of FM4-64 on the DOPC membrane. As depicted in Figure 5F, the histogram obtained from 8 GUVs shows $\overline{D} = 0.45$ in the presence of Ca^{2+} (as opposed to $\overline{D} = 0.5$ in absence of Ca^{2+}, obtained for 8 GUVs). Based on the map in Figure 1, such decrease can be interpreted as a shift to a narrower width of the orientation distribution function of FM4-64 (for $D = 0.4$, values of σ above 48° are not allowed).

Please cite this article in press as: Li et al., On the mechanism and voltage sensitivity of voltage-sensitive second harmonic probes: A case study of FM4-64, Biophysical Journal (2026), https://doi.org/10.1016/j.bpj.2026.07.006

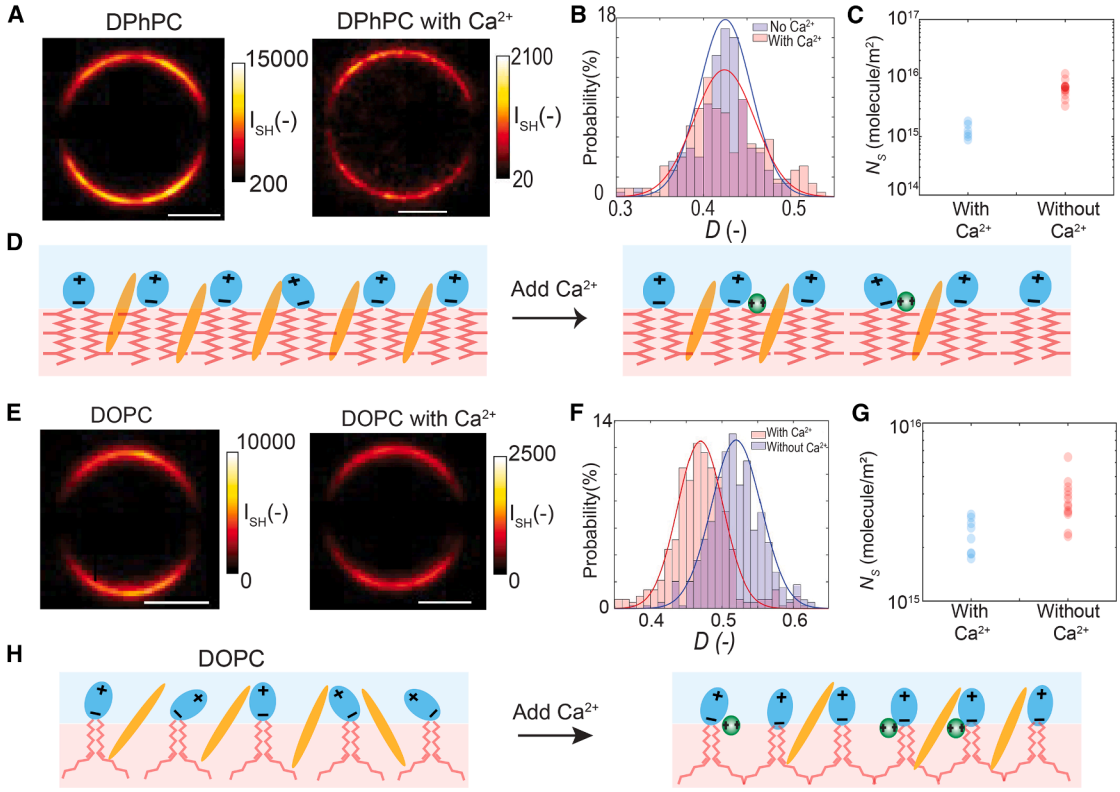

Figure 5. Effects of Ca^{2+} on FM4-64 orientation distribution and surface number density in neutral lipid membranes. The procedure to calculate N_s is detailed in supplemental information S6. (A) SH images of FM4-64-labeled (2 μM) DPhPC GUVs in the absence and presence of 5 mM $CaCl_2$. Scale bar: 20 μm. (B) Corresponding orientational distribution (D values) calculated on 8 GUVs for each case (with and without Ca^{2+}) showing no significant change with Ca^{2+}. (C) Calculated surface number density N_s of FM4-64 on the membrane surface, revealing a decrease upon Ca^{2+} addition. (D) Schematic illustration of Ca^{2+}-induced dye exclusion from the membrane surface. (E) SH images of FM4-64-labeled (2 μM) DOPC GUVs with and without Ca^{2+}. Scale bar: 20 μm. (F) D values analysis on 8 GUVs for each case (with and without Ca^{2+}) yields $\overline{D} = 0.45$ in the presence of Ca^{2+}, pointing to increased lipid ordering. (G) Calculated FM4-64 surface number density N_s on DOPC membranes, also showing a reduction upon Ca^{2+} exposure. (H) Schematic representation of Ca^{2+} effects on DOPC lipid packing and FM4-64 membrane association.

Additionally, in the presence of Ca^{2+}, a decrease in N_s of FM4-64 on the DOPC membrane is also observed, as shown in Figure 5G, although the decrease is less significant than in the DPhPC case (2–3 times decrease). As discussed above, the unsaturated lipid DOPC is likely to have a lower degree of packing order with respect to DPhPC (see Figure 2). Therefore, the decrease of $\overline{D}$ from 0.5 to 0.45 for DOPC is likely to indicate an increase in lipid ordering in this system due to Ca^{2+} binding to the phosphate groups of DOPC lipids. At the same time, Ca^{2+} also results in the decrease of N_s, consistent with the same trend observed in DPhPC GUVs. A schematic representation of these effects, Ca^{2+}-induced lipid ordering and dye exclusion, is provided in Figure 5H. Here, both the FM4-64 surface number density and its ODF are shown to modulate the SH response.

CONCLUSION

In summary, our study highlights the necessity for careful use of VSDs in SH microscopy. Using GUVs as a simplified membrane model system, the SH response of the voltage-sensitive probe FM4-64 and its response in diverse lipid membrane environments is studied. GUVs prepared with different lipids enabled variations in lipid packing and charge, resulting in distinct variations in the SH response of FM4-64. The change in the ODF of the chromophores was quantified by the parameter D, obtained through polarimetric measurements. We first computed the parameter D as a function of the width and mean tilt angle of a Gaussian distribution of VSDs (in three dimensions). D alone does not uniquely determine the orientational distribution but rather defines the range of possible mean tilt angles and distribution widths. We show that values of $D = 0.5$ indicate the possibility that the dye exhibits any orientational distribution going from a strong molecular alignment to a weak one. Such value of D suggests the possible existence of a state in which the inserted dye molecules are only weakly aligned. Conversely, D values above or below 0.5 are representative of a system where the maximum plausible degree of disorder is smaller (i.e., the dye molecules have a higher degree of alignment). For $D \neq 0.5$, we can therefore expect the dye to be inserted in a membrane having a higher degree of packing order.

From polarimetric SH microscopy measurements of electrically neutral GUVs, prepared with DOPC and DPhPC lipids, we find that the unsaturated lipids (DOPC) exhibit a distribution of D values centered at 0.5, pointing to a possibly more disordered membrane than in the case of branched saturated lipids (DPhPC, D values centered at $\overline{D} = 0.42$). The formation of a more disordered membrane in the case of unsaturated lipids is expected from previous X-ray scattering and NMR studies comparing saturated and unsaturated lipids.[51–54] Most importantly, these different values indicate that even in absence of an electro-optic effect due to an electrostatic potential difference, the SH response is affected by the VSD orientational distribution. In charged GUVs, the ODF is directly affected by changes in membrane packing due to variations in the charge density within the membrane. GUVs with an increasingly high content of the charged lipid PA show a distribution of D values centered increasingly closer to 0.5, likely reflecting an increased membrane disorder linked to the repulsion between charged lipid headgroups. Differences in membrane conformation due to charged lipids therefore need to be considered in addition to their direct effect on the electrostatic potential.

Furthermore, we explored how the chemical environment can change the SH response of VSDs, particularly in the presence of Ca^{2+} ions. Our findings indicate that the D values of FM4-64 are modified in the presence of salt in both charged and neutral membranes. For charged membranes, a distribution of lower D values in the presence of Ca^{2+} (D values centered at $\overline{D} = 0.42$ with Ca^{2+}, versus $\overline{D} = 0.51$ without Ca^{2+}) can be explained by the Ca^{2+} binding to the negatively charged phosphate groups and neutralizing the membrane charges, which promotes lipid ordering. For unsaturated lipids, the addition of Ca^{2+} has a similar effect ($\overline{D}$ decreases from 0.5 to 0.45). The decrease in D values upon salt addition on charged membranes and membranes prepared with unsaturated lipids indicates that the range of possible distribution widths has been restricted to favor stronger molecular alignment than in the case of branched saturated lipids ($\overline{D}$ unchanged with Ca^{2+} addition). We additionally quantify the surface number density (N_s) of FM4-64 with and without Ca^{2+} ions on neutral GUVs and demonstrate its decrease in the presence of Ca^{2+}. A reduced incorporation of FM4-64 in the membrane upon Ca^{2+} addition therefore also contributes to changes in the SH signal intensity.

Our findings therefore demonstrate that the SH response is not solely dependent on the VSD electro-optic response induced by variations in any electrostatic potential difference that may affect the membrane, but also significantly influenced by the orientational distribution and the surface number density of the VSD molecules. These factors can lead to much larger variabilities in the SH response, potentially confounding the interpretation of intensity changes if not properly accounted for: variations in chromophore alignment/surface number density can result in disparate SH responses, even under identical voltage conditions. Considering these findings, we conclude that accurate measurement and interpretation of electrostatic potential differences using VSDs in SH microscopy require meticulous calibration and control of any parameter that may influence the orientation distribution function and/or the surface number density of the dye. Addressing these challenges will enhance the reliability and utility of this powerful imaging technique.

DATA AVAILABILITY

The data that support the findings of this study are available from the corresponding author upon reasonable request.

ACKNOWLEDGMENTS

S.R. thanks the Julia Jacobi Foundation, the European Research Council grant agreement no. 951324 (H2020, R2-tension) for financial support. The authors thank Maksim Eremchev and Alex de Beer for helpful discussions.

AUTHOR CONTRIBUTIONS

Z.L., N.A.C.-R., and I.S. collected the experimental data. Z.L. and N.A.C.-R. performed reproducibility validations. Z.L. did the data analysis. Z.L., N.A.C.-R., A.M., S.P., and S.R. analyzed and interpreted the data. Z.L., N.A.C.-R., A.M., and S.R. wrote the manuscript. S.R. conceived and supervised the work. All authors contributed to the article and approved the submitted version.

DECLARATION OF INTERESTS

The authors declare that they have no competing interests.

DECLARATION OF GENERATIVE AI AND AI-ASSISTED TECHNOLOGIES IN THE WRITING PROCESS

The authors acknowledge the use of Grammarly and ChatGPT for assistance in improving the readability and language of the manuscript in parts of the text. The authors remain solely responsible for the scientific content and interpretations presented.

SUPPLEMENTAL INFORMATION

Supplemental information can be found online at https://doi.org/10.1016/j.bpj.2026.07.006.

REFERENCES

1. Chemla, S., and F. Chavane. 2010. Voltage-sensitive dye imaging: Technique review and models. *J. Physiol. Paris.* 104:40–50. https://doi.org/10.1016/j.jphysparis.2009.11.009.

2. Flytzanis, N. C., C. N. Bedbrook, …, V. Gradinaru. 2014. Archaerhodopsin variants with enhanced voltage-sensitive fluorescence in mammalian and Caenorhabditis elegans neurons. *Nat. Commun.* 5:4894. https://doi.org/10.1038/ncomms5894.

Please cite this article in press as: Li et al., On the mechanism and voltage sensitivity of voltage-sensitive second harmonic probes: A case study of FM4-64, Biophysical Journal (2026), https://doi.org/10.1016/j.bpj.2026.07.006

3. Day-Cooney, J., R. Dalangin, …, T. Mao. 2023. Genetically encoded fluorescent sensors for imaging neuronal dynamics in vivo. *J. Neurochem.* 164:284–308. https://doi.org/10.1111/jnc.15608.
4. St-Pierre, F., J. D. Marshall, …, M. Z. Lin. 2014. High-fidelity optical reporting of neuronal electrical activity with an ultrafast fluorescent voltage sensor. *Nat. Neurosci.* 17:884–889. https://doi.org/10.1038/nn.3709.
5. Gong, Y., C. Huang, …, M. J. Schnitzer. 2015. High-speed recording of neural spikes in awake mice and flies with a fluorescent voltage sensor. *Science.* 350:1361–1366. https://doi.org/10.1126/science.aab0810.
6. Yang, W., and R. Yuste. 2017. In vivo imaging of neural activity. *Nat. Methods.* 14:349–359. https://doi.org/10.1038/nmeth.4230.
7. Piatkevich, K. D., S. Bensussen, …, X. Han. 2019. Population imaging of neural activity in awake behaving mice. *Nature.* 574:413–417. https://doi.org/10.1038/s41586-019-1641-1.
8. Bando, Y., M. Wenzel, and R. Yuste. 2021. Simultaneous two-photon imaging of action potentials and subthreshold inputs in vivo. *Nat. Commun.* 12:7229. https://doi.org/10.1038/s41467-021-27444-9.
9. Jin, L., Z. Han, …, V. A. Pieribone. 2012. Single action potentials and subthreshold electrical events imaged in neurons with a fluorescent protein voltage probe. *Neuron.* 75:779–785. https://doi.org/10.1016/j.neuron.2012.06.040.
10. Girouard, S. D., K. R. Laurita, and D. S. Rosenbaum. 1996. Unique properties of cardiac action potentials recorded with voltage-sensitive dyes. *J. Cardiovasc. Electrophysiol.* 7:1024–1038. https://doi.org/10.1111/j.1540-8167.1996.tb00478.x.
11. Grinvald, A., D. Shoham, …, A. Arieli. 1999. In-vivo optical imaging of cortical architecture and dynamics. *In* Modern Techniques in Neuroscience Research Springer, pp. 893–969.
12. Kamino, K., A. Hirota, and S. Fujii. 1981. Localization of pacemaking activity in early embryonic heart monitored using voltage-sensitive dye. *Nature.* 290:595–597. https://doi.org/10.1038/290595a0.
13. Cohen, L. B., B. M. Salzberg, …, C. H. Wang. 1974. Changes in axon fluorescence during activity: Molecular probes of membrane potential. *J. Membr. Biol.* 19:1–36. https://doi.org/10.1007/BF01869968.
14. Dragsten, P. R., and W. W. Webb. 1978. Mechanism of the membrane potential sensitivity of the fluorescent membrane probe merocyanine 540. *Biochemistry.* 17:5228–5240. https://doi.org/10.1021/bi00617a024.
15. Campagnola, P. J., M. D. Wei, …, L. M. Loew. 1999. High-resolution nonlinear optical imaging of live cells by second harmonic generation. *Biophys. J.* 77:3341–3349. https://doi.org/10.1016/S0006-3495(99)77165-1.
16. Campagnola, P. J., and L. M. Loew. 2003. Second-harmonic imaging microscopy for visualizing biomolecular arrays in cells, tissues and organisms. *Nat. Biotechnol.* 21:1356–1360. https://doi.org/10.1038/nbt894.
17. Campagnola, P. J., H. A. Clark, …, L. M. Loew. 2001. Second-harmonic imaging microscopy of living cells. *J. Biomed. Opt.* 63:277–286. https://doi.org/10.1117/1.1383294.
18. Bouevitch, O., A. Lewis, …, L. M. Loew. 1993. Probing membrane potential with nonlinear optics. *Biophys. J.* 65:672–679. https://doi.org/10.1016/S0006-3495(93)81126-3.
19. Peleg, G., A. Lewis, …, L. M. Loew. 1999. Nonlinear optical measurement of membrane potential around single molecules at selected cellular sites. *Proc. Natl. Acad. Sci. USA.* 96:6700–6704. https://doi.org/10.1073/pnas.96.12.6700.
20. Nemet, B. A., V. Nikolenko, and R. Yuste. 2004. Second harmonic imaging of membrane potential of neurons with retinal. *J. Biomed. Opt.* 95:873–881. https://doi.org/10.1117/1.1783353.
21. Loew, L. M., and A. Lewis. 2015. Second Harmonic Imaging of Membrane Potential. *Adv. Exp. Med. Biol.* 859:473–492. https://doi.org/10.1007/978-3-319-17641-3_19.
22. Miller, L. N., W. T. Brewer, …, T. R. Calhoun. 2019. Second Harmonic Generation Spectroscopy of Membrane Probe Dynamics in Gram-Positive Bacteria. *Biophys. J.* 117:1419–1428. https://doi.org/10.1016/j.bpj.2019.09.014.
23. Dombeck, D. A., M. Blanchard-Desce, and W. W. Webb. 2004. Optical recording of action potentials with second-harmonic generation microscopy. *J. Neurosci.* 24:999–1003. https://doi.org/10.1523/JNEUROSCI.4840-03.2004.
24. Sacconi, L., D. A. Dombeck, and W. W. Webb. 2006. Overcoming photodamage in second-harmonic generation microscopy: real-time optical recording of neuronal action potentials. *Proc. Natl. Acad. Sci. USA.* 103:3124–3129. https://doi.org/10.1073/pnas.0511338103.
25. Wilson, S. A., A. Millard, …, L. M. Loew. 2014. Monitoring membrane potential with second-harmonic generation. *Cold Spring Harb. Protoc.* 2014:643–654. https://doi.org/10.1101/pdb.prot081786.
26. Theer, P., W. Denk, …, P. B. Detwiler. 2011. Second-harmonic generation imaging of membrane potential with retinal analogues. *Biophys. J.* 100:232–242. https://doi.org/10.1016/j.bpj.2010.11.021.
27. Nuriya, M., J. Jiang, …, R. Yuste. 2006. Imaging membrane potential in dendritic spines. *Proc. Natl. Acad. Sci. USA.* 103:786–790. https://doi.org/10.1073/pnas.0510092103.
28. Simpson, G. J., and K. L. Rowlen. 1999. An SHG magic angle: Dependence of second harmonic generation orientation measurements on the width of the orientation distribution. *J. Am. Chem. Soc.* 121:2635–2636. https://doi.org/10.1021/ja983683f.
29. Moreaux, L., T. Pons, …, J. Mertz. 2003. Electro-optic response of second-harmonic generation membrane potential sensors. *Opt. Lett.* 288:625–627. https://doi.org/10.1364/ol.28.000625.
30. Simpson, G. J., S. G. Westerbuhr, and K. L. Rowlen. 2000. Molecular orientation and angular distribution probed by angle-resolved absorbance and second harmonic generation. *Anal. Chem.* 72:887–898. https://doi.org/10.1021/ac9912956.
31. Pons, T., L. Moreaux, …, J. Mertz. 2003. Mechanisms of membrane potential sensing with second-harmonic generation microscopy. *J. Biomed. Opt.* 83:428–431. https://doi.org/10.1117/1.1581871.
32. Jiang, J., K. B. Eisenthal, and R. Yuste. 2007. Second Harmonic Generation in Neurons: Electro-Optic Mechanism of Membrane Potential Sensitivity. *Biophys. J.* 93:L26–L28. https://doi.org/10.1529/biophysj.107.111021.
33. Wu, Y., F. L. Yeh, …, E. R. Chapman. 2009. Biophysical Characterization of Styryl Dye-Membrane Interactions. *Biophys. J.* 97:101–109. https://doi.org/10.1016/j.bpj.2009.04.028.
34. Macias-Romero, C., I. Nahalka, …, S. Roke. 2017. Optical imaging of surface chemistry and dynamics in confinement. *Science.* 357:784–788. https://doi.org/10.1126/science.aal4346.
35. Tarun, O. B., C. Hannesschläger, …, S. Roke. 2018. Label-free and charge-sensitive dynamic imaging of lipid membrane hydration on millisecond time scales. *Proc. Natl. Acad. Sci. USA.* 115:4081–4086. https://doi.org/10.1073/pnas.1719347115.
36. Eremchev, M., D. Roesel, …, S. Roke. 2023. High throughput wide field second harmonic imaging of giant unilamellar vesicles. *Biointerphases.* 18:031202. https://doi.org/10.1116/6.0002640.
37. Didier, M. E. P., O. B. Tarun, …, S. Roke. 2018. Membrane water for probing neuronal membrane potentials and ionic fluxes at the single cell level. *Nat. Commun.* 9:5287. https://doi.org/10.1038/s41467-018-07713-w.
38. Millard, A. C., L. Jin, …, L. M. Loew. 2005. Wavelength- and Time-Dependence of Potentiometric Non-linear Optical Signals from Styryl Dyes. *J. Membr. Biol.* 208:103–111. https://doi.org/10.1007/s00232-005-0823-y.
39. Teisseyre, T. Z., A. C. Millard, …, L. M. Loew. 2007. Nonlinear optical potentiometric dyes optimized for imaging with 1064-nm light. *J. Biomed. Opt.* 124:044001. https://doi.org/10.1117/1.2772276.
40. Weinberger, A., F.-C. Tsai, …, C. Marques. 2013. Gel-Assisted Formation of Giant Unilamellar Vesicles. *Biophys. J.* 105:154–164. https://doi.org/10.1016/j.bpj.2013.05.024.
41. Dick, B. 1985. Irreducible Tensor Analysis of Sum-Frequency and Difference-Frequency-Generation in Partially Oriented Samples. *Chem. Phys.* 96:199–215. https://doi.org/10.1016/0301-0104(85)85085-0.

42. Hirose, C., N. Akamatsu, and K. Domen. 1992. Formulas for the Analysis of Surface Sum-Frequency Generation Spectrum by Ch Stretching Modes of Methyl and Methylene Groups. *J. Chem. Phys.* 96:997–1004. https://doi.org/10.1063/1.462120.

43. Zhuang, X., P. B. Miranda, …, Y. R. Shen. 1999. Mapping molecular orientation and conformation at interfaces by surface nonlinear optics. *Phys. Rev. B.* 59:12632–12640. https://doi.org/10.1103/PhysRevB.59.12632.

44. Lambert, A. G., P. B. Davies, and D. J. Neivandt. 2005. Implementing the theory of sum frequency generation vibrational spectroscopy: A tutorial review. *Appl. Spectrosc. Rev.* 40:103–145. https://doi.org/10.1081/Asr-200038326.

45. Reeve, J. E., H. L. Anderson, and K. Clays. 2010. Dyes for biological second harmonic generation imaging. *Phys. Chem. Chem. Phys.* 12:13484–13498. https://doi.org/10.1039/c003720f.

46. Wang, H. F., L. Velarde, …, L. Fu. 2015. Quantitative sum-frequency generation vibrational spectroscopy of molecular surfaces and interfaces: lineshape, polarization, and orientation. *Annu. Rev. Phys. Chem.* 66:189–216. https://doi.org/10.1146/annurev-physchem-040214-121322.

47. Guyot-Sionnest, P., J. H. Hunt, and Y. R. Shen. 1987. Sum-frequency vibrational spectroscopy of a Langmuir film: Study of molecular orientation of a two-dimensional system. *Phys. Rev. Lett.* 59:1597–1600. https://doi.org/10.1103/PhysRevLett.59.1597.

48. Roy, S., P. A. Covert, …, D. K. Hore. 2014. Biomolecular structure at solid-liquid interfaces as revealed by nonlinear optical spectroscopy. *Chem. Rev.* 114:8388–8415. https://doi.org/10.1021/cr400418b.

49. Simpson, G. J., and K. L. Rowlen. 1999. Quantification of "local" surface orientation: Theory and experiment. *J. Phys. Chem. B.* 103:1525–1531. https://doi.org/10.1021/jp983396y.

50. Quinn, P. J., F. Joo, and L. Vigh. 1989. The role of unsaturated lipids in membrane structure and stability. *Prog. Biophys. Mol. Biol.* 53:71–103. https://doi.org/10.1016/0079-6107(89)90015-1.

51. Koenig, B. W., H. H. Strey, and K. Gawrisch. 1997. Membrane lateral compressibility determined by NMR and x-ray diffraction: effect of acyl chain polyunsaturation. *Biophys. J.* 73:1954–1966. https://doi.org/10.1016/S0006-3495(97)78226-2.

52. Kučerka, N., S. Tristram-Nagle, and J. F. Nagle. 2006. Structure of fully hydrated fluid phase lipid bilayers with monounsaturated chains. *J. Membr. Biol.* 208:193–202. https://doi.org/10.1007/s00232-005-7006-8.

53. Tristram-Nagle, S., D. J. Kim, …, J. F. Nagle. 2010. Structure and water permeability of fully hydrated diphytanoylPC. *Chem. Phys. Lipids.* 163:630–637. https://doi.org/10.1016/j.chemphyslip.2010.04.011.

54. Marsh, D. 2013. Handbook of Lipid Bilayers. CRC press.

55. Nagle, J. F., and S. Tristram-Nagle. 2000. Structure of lipid bilayers. *Biochim. Biophys. Acta Rev. Biomembr.* 1469:159–195. https://doi.org/10.1016/s0304-4157(00)00016-2.

56. Lindsey, H., N. O. Petersen, and S. I. Chan. 1979. Physicochemical characterization of 1,2-diphytanoyl-sn-glycero-3-phosphocholine in model membrane systems. *Biochim. Biophys. Acta.* 555:147–167. https://doi.org/10.1016/0005-2736(79)90079-8.

57. Redwood, W. R., F. R. Pfeiffer, …, T. E. Thompson. 1971. Physical properties of bilayer membranes formed from a synthetic saturated phospholipid in n-decane. *Biochim. Biophys. Acta.* 233:1–6. https://doi.org/10.1016/0005-2736(71)90351-8.

58. Srivastava, A., and K. B. Eisenthal. 1998. Kinetics of molecular transport across a liposome bilayer. *Chem. Phys. Lett.* 292:345–351. https://doi.org/10.1016/S0009-2614(98)00662-9.

59. Moreaux, L., O. Sandre, …, J. Mertz. 2001. Coherent Scattering in Multi-Harmonic Light Microscopy. *Biophys. J.* 80:1568–1574. https://doi.org/10.1016/S0006-3495(01)76129-2.

60. Li, Z., I. Swiderska, …, S. Roke. 2025. Membrane potential fluctuations and water asymmetry on plasma cell and model lipid membranes: origins, implications and properties. *Faraday Discuss.* 259:342–365. https://doi.org/10.1039/d4fd00197d.

61. Swiderska, I., S. Lee, …, S. Roke. 2026. Second harmonic imaging of membrane potentials: comparing water and chromophores as probes. *Biophys. J.* 11:S0006. https://doi.org/10.1016/j.bpj.2026.06.014.